NASA/TM–2012-216048

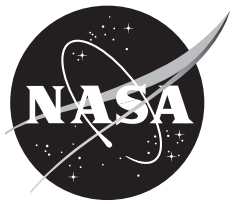

Boeing SMART Rotor Full-Scale Wind Tunnel Test Data Report

Brandon Hagerty
Universities Space Research Association
Ames Research Center
Moffett Field, California

Sesi Kottapalli
Ames Research Center
Moffett Field, California

October 2012

The NASA STI Program Office . . . in Profile

Since its founding, NASA has been dedicated to the advancement of aeronautics and space science. The NASA Scientific and Technical Information (STI) Program Office plays a key part in helping NASA maintain this important role.

The NASA STI Program Office is operated by Langley Research Center, the Lead Center for NASA's scientific and technical information. The NASA STI Program Office provides access to the NASA STI Database, the largest collection of aeronautical and space science STI in the world. The Program Office is also NASA's institutional mechanism for disseminating the results of its research and development activities. These results are published by NASA in the NASA STI Report Series, which includes the following report types:

- TECHNICAL PUBLICATION. Reports of completed research or a major significant phase of research that present the results of NASA programs and include extensive data or theoretical analysis. Includes compilations of significant scientific and technical data and information deemed to be of continuing reference value. NASA's counterpart of peer-reviewed formal professional papers but has less stringent limitations on manuscript length and extent of graphic presentations.

- TECHNICAL MEMORANDUM. Scientific and technical findings that are preliminary or of specialized interest, e.g., quick release reports, working papers, and bibliographies that contain minimal annotation. Does not contain extensive analysis.

- CONTRACTOR REPORT. Scientific and technical findings by NASA-sponsored contractors and grantees.

- CONFERENCE PUBLICATION. Collected papers from scientific and technical conferences, symposia, seminars, or other meetings sponsored or cosponsored by NASA.

- SPECIAL PUBLICATION. Scientific, technical, or historical information from NASA programs, projects, and missions, often concerned with subjects having substantial public interest.

- TECHNICAL TRANSLATION. English-language translations of foreign scientific and technical material pertinent to NASA's mission.

Specialized services that complement the STI Program Office's diverse offerings include creating custom thesauri, building customized databases, organizing and publishing research results . . . even providing videos.

For more information about the NASA STI Program Office, see the following:

- Access the NASA STI Program Home Page at *http://www.sti.nasa.gov*

- E-mail your question via the Internet to help@sti.nasa.gov

- Fax your question to the NASA Access Help Desk at (301) 621-0134

- Telephone the NASA Access Help Desk at (301) 621-0390

- Write to:
  NASA Access Help Desk
  NASA Center for AeroSpace Information
  7115 Standard Drive
  Hanover, MD 21076-1320

NASA/TM–2012-216048

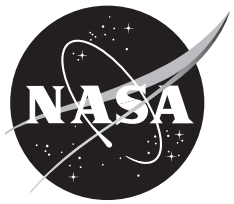

Boeing SMART Rotor Full-Scale Wind Tunnel Test Data Report

Brandon Hagerty
Universities Space Research Association
Ames Research Center
Moffett Field, California

Sesi Kottapalli
Ames Research Center
Moffett Field, California

National Aeronautics and
Space Administration

Ames Research Center
Moffett Field, California 94035-1000

October 2012

Available from:

NASA Center for AeroSpace Information
7115 Standard Drive
Hanover, MD 21076-1320
(301) 621-0390

National Technical Information Service
5285 Port Royal Road
Springfield, VA 22161
(703) 487-4650

TABLE OF CONTENTS

DATA DVD (attached):

LIST OF FIGURES

LIST OF TABLES

NOMENCLATURE

ALFSC	corrected angle of attack, Boeing data, + aft tilt (deg)
COLLA	rotor collective control input, + nose up (deg)
C_P	rotor power coefficient (equivalent to torque coefficient)
CPOS	rotor power coefficient over solidity, C_P/σ
CSND	tunnel speed of sound, ft/s
C_T	rotor thrust coefficient, + up
CTHHC	Continuous Time Higher Harmonic Controller
CTOS	rotor thrust coefficient over solidity, C_T/σ, + up
DRAGRH	rotor drag force, obtained from rotor balance, corrected for weight tare and shaft rotation tare, + aft (lbf)
Harmonics	flap frequency in cycles per rotor revolution
HP	horsepower from rotor torque
LATA	rotor lateral control input, nose down at PSI = 0^o (deg)
LONGA	rotor longitudinal control input, nose down at PSI = 90^o (deg)
MAT	rotor advancing tip Mach number
MTIP	rotor tip Mach number
MTUN	tunnel Mach number
MU	rotor advance ratio, tunnel speed/OMR
n	harmonic index (0 to N) or harmonic frequency n/rev, also nP
OMR	rotor tip speed (ft/s)
PITCHRH	rotor pitch moment obtained from rotor balance, corrected for weight tare and shaft rotation tare, + nose up (in-lbf)
PS	static pressure at tunnel centerline (psfa)
Q	corrected tunnel dynamic pressure (psf)
RDMS	Rotor Data Management System
RHO	air density ($slug/ft^3$)
ROLLRH	rotor roll moment obtained from rotor balance, corrected for weight tare and shaft rotation tare, + right side down (in-lbf)
RPM	rotor RPM, + counterclockwise from top
SIDERH	rotor side force obtained from rotor balance, corrected for weight tare and shaft rotation tare, + right (lbf)
THRUST	rotor thrust force parallel to rotor shaft, + up (lbf)
TORQ	rotor torque, + drag (in-lbf)
TSR	tunnel static temperature (deg_R)
VISC	tunnel air viscosity (slug/ft-s)
VKTS	tunnel speed (knots)
α_{su}	uncorrected shaft angle-of-attack, + aft tilt (deg)
σ	rotor solidity, blade area/disc area

BOEING SMART ROTOR FULL-SCALE WIND TUNNEL TEST DATA REPORT

Brandon Hagerty[1] and Sesi Kottapalli

NASA Ames Research Center

SUMMARY

A full-scale helicopter smart material actuated rotor technology (SMART) rotor test was conducted in the NASA Ames 40- by 80-Foot Wind Tunnel. The SMART rotor system is a five-bladed MD 902 bearingless rotor with active trailing-edge flaps. The flaps are actuated using piezoelectric actuators. Rotor performance, structural loads, and acoustic data were obtained over a wide range of rotor shaft angles of attack, thrust, and airspeeds. The primary test objective was to acquire unique validation data for the high-performance computing analyses developed under the Defense Advanced Research Project Agency (DARPA) Helicopter Quieting Program (HQP). Other research objectives included quantifying the ability of the on-blade flaps to achieve vibration reduction, rotor smoothing, and performance improvements. This data set of rotor performance, structural loads, and rotor flap frequency sweep (chirp) tests can be used for analytical and experimental comparison studies with other full-scale rotor systems and for analytical validation of computer simulation models. The purpose of this final data report is to document a comprehensive, high-quality data set that includes only data points where the flap was actively controlled and each of the five flaps behaved in a similar manner.

INTRODUCTION

The Boeing Company developed the SMART rotor under a DARPA smart materials and structures demonstration program. The objectives of the SMART rotor program were to demonstrate smart materials for active control on a helicopter rotor and quantify performance and cost benefits. Piezoelectric actuators, driving trailing-edge flaps on a modified MD 902 rotor, were used to reduce vibration and noise, improve aerodynamic performance, and perform other active control functions. Development of the actuation and rotor system was supported by DARPA. NASA and the U.S. Army funded fabrication of the rotor blades. The state-of-the-art five-bladed composite bearingless main rotor system of the MD 902 was modified to include on-blade piezoelectric actuators and trailing-edge flaps. The MD 902 Explorer twin engine, light-utility helicopter is the intended flight demonstration vehicle for a future, anticipated flight test.

[1] Universities Space Research Association, NASA Ames Research Center, Moffett Field, CA 94035.

1992 MDART Rotor Test

The McDonnell Douglas Helicopter Company (MDHC) and NASA Ames Research Center jointly conducted a test of the McDonnell Douglas Advanced Rotor Technology (MDART) rotor in the Ames 40- by 80-Foot Wind Tunnel in 1992. The MDART rotor is a modern, five-bladed bearingless design that incorporates elastomeric dampers to augment the damping of the blade in-plane motion. This test was the first wind tunnel test of a full-scale, five-bladed bearingless rotor. It was also the first test to apply higher harmonic control (HHC) to a full-scale bearingless rotor in order to study the effect of HHC on rotor vibration, loads, and noise. Prior to the wind tunnel test, the MDART rotor underwent hover testing at the Boeing Mesa whirl stand (ref. 1). The objective of the MDART wind tunnel test program was to evaluate the aerodynamic performance and aeromechanic properties of the MDART rotor. MDART testing at Ames Research Center provided a significant amount of performance, loads, and stability data up to airspeeds of 200 knots and thrusts of 1.8g (refs. 2–3). The measurements were compared with predictions from the University of Maryland Advanced Rotorcraft Code (UMARC) in order to improve computational prediction tools (ref. 4). The results from this 1992 wind tunnel test can be considered as a baseline data set for an unmodified MD 900 rotor.

Differences between the MDART rotor and the recent Boeing SMART rotor designs include blade spar modifications to incorporate the on-blade flaps and smart material actuators, as well as slight modifications to the flexbeams (ref. 5).

DESCRIPTION OF EXPERIMENT

A modified full-scale MD 902 Explorer rotor with on-blade piezoelectric-actuated trailing-edge flaps was used to demonstrate the capabilities of active-flap technology in forward flight. The objective of the DARPA program was to demonstrate the impact of active flaps on rotor acoustics for the purpose of establishing a validation database for noise prediction tools (ref. 6). The HQP program was initiated in 2004 to develop high-fidelity state-of-of-the-art computational tools necessary for designing advanced helicopter rotors with reduced acoustic perceptibility and enhanced performance. A critical step towards this achievement is the development of rotorcraft prediction codes capable of assessing a wide range of helicopter configurations and operations for future rotorcraft designs. This includes novel next-generation rotor systems that incorporate innovative passive and/or active elements to meet future challenging military performance and survivability goals. Wind tunnel testing was successfully and safely concluded in 2008, meeting all DARPA HQP high-priority objectives (refs. 7–13).

Under supplemental NASA funding, additional wind tunnel testing was conducted to demonstrate and quantify vibration, noise, and performance improvements. The authority, effectiveness, and reliability of the flap actuation system were demonstrated in 65 hours of testing at up to 155 knots airspeed and 7,700 lb thrust. Validation data was successfully acquired for all test conditions. The effectiveness of the flap for noise and vibration control was demonstrated conclusively, with the results showing significant reductions in blade-vortex interaction (BVI) and in-plane noise, as well as vibratory hub loads; the impact of the flap on control power and rotor smoothing was also demonstrated (refs. 8–15). References 16–19 list relevant Boeing technical reports.

Test Setup

The 11-week-long test in the National Full-Scale Aerodynamics Complex (NFAC) was conducted between February and April 2008. The SMART rotor was installed on Boeing's Large Rotor Test Stand (LRTS) with the rotor hub 23.8 ft above the acoustic lining of the tunnel floor (figs. 1 and 2). The LRTS was supported by two main front struts and a telescoping tail strut. Tail-strut retraction provided shaft angle-of-attack adjustment. Connected by the vertical test-stand strut, the LRTS consisted of a lower and an upper housing. The lower housing enclosed a 1,500-HP General Electric motor and transmission. The upper housing enclosed the rotor balance and hydraulic servo-actuators for the rotor primary control system. A five-component rotor balance was mounted on top of a static mast that connected to the rotor hub in the upper housing. The balance measured three forces (lift, drag, and side) and two moments (pitch and roll). Torque was passed directly to the rotor hub through the rotating drive shaft that was confined in the static mast. Rotor torque was measured on the flex coupling between the drive shaft and the rotor.

Test Hardware

The five-bladed SMART bearingless rotor is 33.85 ft in diameter and has an HH-10 (12-percent-thick) airfoil at the in-board section and an HH-06 (9.5-percent-thick) airfoil at the outboard section. The blade region from 0.93R to the tip has a parabolic leading edge sweep (22 deg at the tip) with straight trailing edge and a 2:1 taper ratio. The active flap extends from 0.74R to 0.92R and has a flap chord of 25-percent blade chord (hinge to trailing edge) with an overhang of 40 percent, resulting in a total flap chord that is 35 percent of blade chord. The piezoelectric actuators, embedded in the blade spar, are centered at 0.74R. The actuators are designed to drive the trailing-edge flap frequencies up to 6/rev (6P) with maximum amplitude of ±3 deg. Rotor characteristics are given in table 1.

Piezoelectric On-Blade Actuators

The piezoelectric actuators consist of two X-frame mechanisms and four piezoelectric stack columns. The two X-frames are mechanically in parallel, in a push-pull configuration, thus the forces add up and displacements are constrained to be identical. The stack columns in each X-frame are mechanically and electrically preloaded to always be in compression. Applying a positive voltage to the two stack columns extends their length, reducing the enclosed angle and closing the X-frame mechanism. Flap motion control is typically achieved by supplying bias (0 to 10V DC) and dynamic (0 ±10V AC) voltage commands to the amplifier. The drive voltages for the two channels, i.e., inboard and outboard X-frame actuator, are set 180 deg out of phase. The bias voltage contributes to the actuator preload but ideally produces no flap deflection. The flap deflection is proportional to the dynamic voltage. Flap actuator operations were limited to a dynamic voltage of 400 ±500V with a relative humidity (RH) < 55 percent, and 400 ±600V with RH < 45 percent. The flap range of motion was ±3 deg and was measured by a Hall effect sensor. Positive flap deflection is defined as trailing-edge down. Flap actuator characteristics are given in table 1.

Data Channels

In addition to the microphone and rotor-balance measurements, other measurements were also made using rotating-blade, stationary, and wind-tunnel channels. Blade #1, the primary blade, was fully instrumented with rotating-blade channels that included flap, lag, and torsional strain gauges on the flexbeam, pitchcase, and blade at various spanwise stations (fig. 3). During the test, the critical flexbeam flap-bending gauge at $r/R = 0.044$ (station 9) was used by the rotor operator to minimize blade 1P flapping (and hence 1P hub moments) at the desired test point; an active backup gauge (channel) was also used on blade #2 at the same station, $r/R = 0.044$. Other rotating system channels included the active-flap position (each blade) measured through a linear voltage differential transformer (LVDT) sensor, and the input voltage and current to the piezoelectric actuators. The stationary channels included the nonrotating swashplate position, the rotor speed, the test-stand vibration, and the inter-range instrumentation group B (IRIG-B) time code.

The standard wind-tunnel channels included the model shaft angle of attack, temperature, pressure, humidity, etc. Additional channels for derived quantities like air density, advance ratio, rotor collective, etc., used data from the standard wind-tunnel channels.

Microphones

During the Boeing SMART rotor test, a set of microphones was strategically placed around the model to capture rotor noise sources of interest. These microphones (figs. 2 and 4) were grouped into: a) out-of-plane fixed microphones (M1 and M4) to correlate to microphones used previously in the MDART test; b) traverse microphones (M5 through M12) that could be moved along guided rails for out-of-plane BVI noise mapping; and c) in-plane microphones (M13, M14, and M15) for low-frequency, in-plane rotor noise measurement. Microphones M13, M14, and M15 were mounted on tower struts to be near the plane of the rotor (in-plane, approximately 10 deg below wind-tunnel centerline). These microphones were also intentionally positioned along a straight line originating from the advancing blade tip to the tunnel centerline to help determine the near-field/far-field characteristics of in-plane rotor noise. With the exception of M14, all microphones were located within the acoustically treated portion of the 40- by 80-Foot Wind Tunnel test section. To account for non-zero shaft tilt angle, the microphone coordinates must be transformed accordingly using the pivot point located 163 inches below the rotor hub. Acoustic data are presented in a separate report and are not included herein.

Data Acquisition Systems and Post-Test Data Processing

The SMART test used two sets of data acquisition systems: the NFAC wind tunnel data system and the Boeing pulse-code modulation (PCM) data system. The 12-bit Boeing data system consisted of a rotating and a stationary unit. The stationary data unit mounted on top aft of the right main strut was responsible for acquiring all stationary channels, the wind-tunnel channels, the traverse microphone channels, and a reference channel. The rotating data unit enclosed in a circular fairing on top of the rotor hub acquired all rotating channels and transmitted them through slip rings. Both units provided signal conditioning to the sensors, and sampled and transmitted the digital data as PCM streams at 10 Mb/s. The PCM streams were then combined and recorded on a digital tape and a computer in the

wind-tunnel control room. The Boeing system acquired all data continuously at fixed sampling rates, mostly at 1250 Hz but some at 0.3333, 625, 3750, 10k, and 15k Hz.

Unlike Boeing's time-base data system, the NFAC data system acquired all data simultaneously at two rotor-synchronized rates: 256 samples/rev for wind-tunnel channels and 2048 samples/rev for all (AC-coupled) microphone channels. For each test point, 64 revolutions of data (about 9.8 sec) were recorded. Synchronized azimuth-based sampling allows the extraction of exceptional signal-to-noise ratios associated with the rotational harmonics of the rotor. Any fluctuations not associated with the rotor harmonic frequencies are naturally suppressed by the azimuth-based technique when averaged over all 64 revolutions of data.

Post-test data processing for the Boeing data involved more steps than for the NFAC data. The reference channel (a 0.2-Hz triangle signal) was used as the time alignment reference between the Boeing and the NFAC data systems. Then 64 revolutions of Boeing data were extracted for processing, and corrected for time shifting due to the sequential sampling of the PCM systems and the 7-deg offset of the 1/rev encoder. The Boeing data was then spline-fitted to 256 samples/rev and converted from raw counts into engineering units. Phase correction for the anti-aliasing filter was also applied and then stored on the NASA Ames Rotor Data Management System (RDMS) data server. Because NFAC data were sampled simultaneously and synchronously with the rotor speed, the only correction to the NFAC data was the 7-deg offset of the 1/rev encoder. After the Boeing and the NFAC data were merged together onto the RDMS server, weight and aerodynamic hub tare corrections were applied to the rotor balance data. As noted earlier, blade #1 is the fully instrumented blade and each succeeding blade is labeled in order from 2 to 5; when blade #1 is directly over the "tail" (i.e., pointing downstream) the rotor is at 0-deg azimuth.

Rotor Data Management System (RDMS)

At Ames Research Center, the RDMS is the storage system for wind tunnel test data. Created by Randy Peterson, RDMS provides both corrected and uncorrected data. Data is corrected using weight and aerodynamic tares as shown in table 2.

DATA ANALYSIS

The purpose of this data report is to document a comprehensive, high-quality data set. This data report considers only those data points where the flaps were actively controlled. In order to identify (and analyze) the relevant data of present interest, the RDMS SMART rotor test data set was selectively narrowed down. An initial review of all the data showed that the flap controller was working correctly as designed during runs 42–64. Starting with these runs, approximately 1400 test points were considered for detailed analysis. These 1400 points were further narrowed down to approximately 550 points through the imposition of flap deflection and phase constraints, described as follows and summarized in table 3:

i) The first step was to remove points with *thrust* < 100 lb. This was done to eliminate points where the rotor was not spinning.

ii) The second constraint was to exclude points with *airspeed* < 10 knots. This separated hover points from forward-flight points.

iii) The next step was to eliminate points that showed blade-to-blade differences in the *mean values of the flap deflection*, with blade #1 as the reference blade. The mean flap deflection of each blade was subtracted from the mean flap deflection of blade #1. This gave the differences in mean values for blades 2, 3, 4, and 5. After a close study of the data, a mean difference of 0.3 deg for all blades was considered to be acceptable; all points that had a blade with a mean difference magnitude > 0.3 deg were eliminated.

iv) Blade-to-blade differences in *maximum flap deflection* were handled in a manner similar to iii) above with the following exception. For the maximum flap deflection it was observed that the data could be split into the following two groups (ranges): a maximum flap amplitude range of 0–1.3 deg and 1.3–3.0 deg. The tolerance for the first group, 0–1.3 deg, was found to be ±0.15 deg between each blade (2 to 5, relative to blade #1). The corresponding tolerance for the second group, 1.3–3 deg, was found to be ±0.21 deg. Splitting the data set into these two groups allowed the more accurate control of the flaps at lower amplitudes to be easily seen. Blade-to-blade differences in *minimum flap deflection* were handled in the same manner as described above with the same numerical values for the two groups, etc.

v) After the flap displacement criteria were implemented and relevant points removed from the data set considered for this report, the *phase angle* was considered. The phase angle depends on the commanded (driven) harmonic amplitude and the corresponding measured individual flap deflection; that is, the phase angle is the difference between the commanded and measured flap harmonic amplitudes. The phase angle was corrected for the blade-to-blade 72-deg-azimuth shift. For commanded harmonic amplitudes > 0.1 deg, a phase angle tolerance of ±0.5 deg was established. This criterion was only used on data points where there was an active input; the 0-deg deflection cases were not subject to this criterion. All multiple harmonic points such as those associated with the vibration reduction part of the data set were subject to this criterion (for all commanded harmonics).

PRESENTED DATA

Overall, Appendix A contains summaries of specific tests and Appendices B through K contain data. The names, descriptions, units, and positive directions of the data channels referred to in the main text are listed under Nomenclature. The other remaining channels, the Static Data and Dynamic Data channels, are shown in tables 4 and 5, respectively. The contents of tables 4 and 5 are also included in all appendices. In tables 4 and 5, the channels are listed in the order that they appear in the data appendices, not alphabetically. In the data appendices, static data is represented by the mean value of the parameter under consideration and, separately, dynamic data is represented by 15 harmonics. The equation for the dynamic data is as follows:

$$\text{Dynamic data value} = a0 + a1c*\cos(psi) + b1s*\sin(psi) + a2c*\cos(2psi) + b2s*\sin(2psi)\ldots$$

where psi is the azimuth angle and psi = 0 deg when blade #1 is directly over the tail, i.e., pointing downstream, and a0, a1c, b1s, etc., are the harmonic coefficients given in the dynamic data appendices. The data appendices contain mutually exclusive data associated with particular test conditions.

The data presented in this report is arranged primarily by airspeed, and within the airspeed groupings the data points are arranged by their commanded harmonics (i.e., the commanded harmonic input to the flap). Within each harmonic grouping, the data points are arranged by ascending run and point number. Along with this arrangement of data, the dynamic and static channels that provide a more in-depth description of each run point are also given. The additional description channels include the rotor thrust, rotor RPM, balance forces and moments, control inputs, and environmental conditions. A data DVD is attached to this report; it contains the full time-history records of the listed channels for all the data points in this report.

TABLE 1. BOEING SMART ROTOR AND ACTIVE FLAP CHARACTERISTICS

Rotor	
Rotor	Modified MD 902
Hub type	Bearingless
Number of blades	5
Radius, ft	16.925
Blade chord, ft	0.8333
Airfoil	HH-10, t/c = 12%; r/R < 0.74 HH-06, t/c = 9.5%; 0.74 < r/R < 0.84
Tip sweep	Parabolic leading edge, 0.93 < r/R < 1; 22 at tip
Tip taper	2:1 straight trailing edge
Twist rate	–10
Rotor solidity	0.075
Nominal rotor speed, rpm	392
Nominal tip speed, ft/s	695
Nominal thrust, lbf	5811
Nominal C_T/σ	0.075
Active Flap	
Radial span	0.74 < r/R < 0.92
Total chord	0.35c
Hinge location	0.75c
Flap twist axis	1.0 in aft of flap leading edge
Control horn length, ft	0.75
Maximum flap angle	±3
Flap weight, lbm	1.26

TABLE 2. WEIGHT AND AERODYNAMIC TARES

Tare Type	Parameters	Balance Application	VKTS	RPM	Shaft Angle			Blades
					Min	Max	Delta	
Weight Tare, Hub Only	Shaft angle	Rotor, scale	0	0	–15	10	2.5	off
Rotation Tare	Shaft angle, RPM	Rotor	0	392	–15	10	2.5	off
Aero Tare	Shaft angle, Q	Rotor, scale	20	392	–5	0	2.5	off
Aero Tare	Shaft angle, Q	Rotor, scale	40	392	–5	0	2.5	off
Aero Tare	Shaft angle, Q	Rotor, scale	60	392	–5	10	2.5	off
Aero Tare	Shaft angle, Q	Rotor, scale	120	392	–15	10	2.5	off
Aero Tare	Shaft angle, Q	Rotor, scale	150	392	–15	10	2.5	off
Weight Tare, Hub and Blades	Shaft angle	Rotor, scale	0	0	–15	10	2.5	on
Post Test Aero Tare	Shaft angle = 0, Q	Rotor, scale	0-150	392	0			off

TABLE 3. PARAMETERS AND CONSTRAINTS USED IN DATA SELECTION AND ANALYSIS

Data Set Parameter	Constraint
i) Thrust	Thrust < 100 lb
ii) Airspeed	Airspeed < 10 knots
iii) Flap mean deflection	$\pm 0.3^{o}$
iv) Flap max deflection group 1, amp 0^{o}–1.3^{o}	$\pm 0.15^{o}$
Flap max deflection group 2, amp 1.3^{o}–3^{o}	$\pm 0.21^{o}$
Flap min deflection group 1, amp 0^{o}–1.3^{o}	$\pm 0.15^{o}$
Flap min deflection group 2, amp 1.3^{o}–3^{o}	$\pm 0.21^{o}$
v) Phase angle, amp > 0.1^{o}	$\pm 0.5^{o}$

TABLE 4. STATIC DATA PARAMETERS AND DESCRIPTIONS

Channel Name	Description	Units	Positive Direction
VKTS	Tunnel speed	kt	
ALFSC	Corrected angle of attack, Boeing data	deg	aft
HP	Horsepower from rotor torque	HP	
THRUST	Rotor thrust force parallel to the rotor shaft, shaft axes system	lbf	up
COLLA	Rotor collective control input, obtained from the actuator A set of LVDTs, positive nose up	deg	nose up
MTUN	Tunnel Mach number		
CTOS	Rotor thrust coefficient over solidity, parallel to the rotor shaft, shaft axes system		up
LATA	Rotor lateral control input, obtained from the actuator A set of LVDTs, positive nose down at PSI = 0 deg	deg	nose down at PSI = 0 deg
MU	Rotor advance ratio		
MTIP	Tip Mach number		
Flap 1 Amp	Flap 1 maximum angle	deg	t.e. down
LONGA	Rotor longitudinal control input, obtained from the actuator A set of LVDTs, positive nose down at PSI = 90 deg	deg	nose down at PSI = 90 deg
OMR	Rotor tip speed	ft/s	CCW from top
MAT	Rotor advancing tip Mach number		
RPM	Rotor rpm	rpm	CCW from top
ROLLRH	Rotor roll moment obtained from the rotor balance, corrected for weight tare and shaft rotation tare	in-lbf	right down
Flap 1 Phase	Phase angle flap 1 began	deg	CCW zero over tail
PS	Static pressure at tunnel centerline	psfa	
PITCHRH	Rotor pitch moment obtained from the rotor balance, corrected for weight tare and shaft rotation tare	in-lbf	nose up
Flap 1 Harm	Harmonic/s induced into flap controller		
RHO	Air density	$slug/ft^3$	
TORQ	Rotor torque	in-lbf	drag
Q	Corrected tunnel dynamic pressure	psf	
TSR	Tunnel static temperature	deg_R	
SIDERH	Rotor side force obtained from the rotor balance, corrected for weight tare and shaft rotation tare	lbf	right
CSND	Tunnel speed of sound	ft/s	
VISC	Tunnel air viscosity	slug/ft-sec	
DRAGRH	Rotor drag force obtained from the rotor balance, corrected for weight tare and shaft rotation tare	lbf	aft
CPOS	Rotor power coefficient over solidity		

TABLE 5. DYNAMIC DATA PARAMETERS AND DESCRIPTIONS

Channel Name	Description	Units	Positive Direction
FLAP1C	Flap 1 Angle (corrected)	deg	t.e. down
ACT1DISP	MR Flap Actuator1 Displacement (feedback), Sta 150	V	aft
ACT1FORCE	MR Flap Actuator1 Force (flap link), Sta 150	lbf	compression
FA1IBCURRENT	Flap Actuator1 Inboard Current	A	
FA1IBVOLTAGE	Flap Actuator1 Inboard Voltage	V	
FA1OBCURRENT	Flap Actuator1 Outboard Current	A	
FA1OBVOLTAGE	Flap Actuator1 Outboard Voltage	V	
MRBLD1CB42P75	MR Blade 1 Chord Bending Sta 42.75	in-lbf	lag
MRBLD1CB70	MR Blade 1 Chord Bending Sta 70	in-lbf	lag
MRBLD1CB120	MR Blade 1 Chord Bending Sta 120	in-lbf	lag
MRBLD1CB164	MR Blade 1 Chord Bending Sta 164	in-lbf	lag
MRBLD1FB42P75	MR Blade 1 Flap Bending Sta 42.75	in-lbf	tip up
MRBLD1FB70	MR Blade 1 Flap Bending Sta 70	in-lbf	tip up
MRBLD1FB87	MR Blade 1 Flap Bending Sta 87	in-lbf	tip up
MRBLD1FB120	MR Blade 1 Flap Bending Sta 120	in-lbf	tip up
MRBLD1FB164	MR Blade 1 Flap Bending Sta 164	in-lbf	tip up
MRBLD1FB180	MR Blade 1 Flap Bending Sta 180	in-lbf	tip up
MRBLD1TOR51	MR Blade 1 Torsion Sta 51	in-lbf	le up
MRBLD1TOR71	MR Blade 1 Torsion Sta 71	in-lbf	le up
MRBLD1TOR130	MR Blade 1 Torsion Sta 130	in-lbf	le up
MRBLD1TOR164	MR Blade 1 Torsion Sta 164	in-lbf	le up
MRFBM1CB26P5	MR Flexbeam 1 Chord Bending Sta 26.5	in-lbf	lag
MRFBM1FB9	MR Flexbeam 1 Flap Bending Sta 9	in-lbf	tip up
MRFBM1TOR26P5	MR Flexbeam 1 Torsion Sta 26.5	in-lbf	le up
MRPC1CB33P25	MR Pitchcase 1 Chord Bending Sta 33.25	in-lbf	lag
MRPC1FB33P25	MR Pitchcase 1 Flap Bending Sta 33.25	in-lbf	tip up
MRPC1TOR25P5	MR Pitchcase 1 Torsion Sta 25.5	in-lbf	le up
MRPLK1LOAD	MR Pitchcase 1 Pitchlink Load	lbf	tension
PITCHRH	Rotor pitch moment obtained from the rotor balance, corrected for weight tare and shaft rotation tare	in-lbf	nose up
ROLLRH	Rotor roll moment obtained from the rotor balance, corrected for weight tare and shaft rotation tare	in-lbf	right down
TORQ	Rotor torque	in-lbf	drag
THRUST	Rotor thrust force parallel to the rotor shaft, shaft axes system	lbf	up
SIDERH	Rotor side force obtained from the rotor balance, corrected for weight tare and shaft rotation tare	lbf	right
DRAGRH	Rotor drag force obtained from the rotor balance, corrected for weight tare and shaft rotation tare	lbf	aft

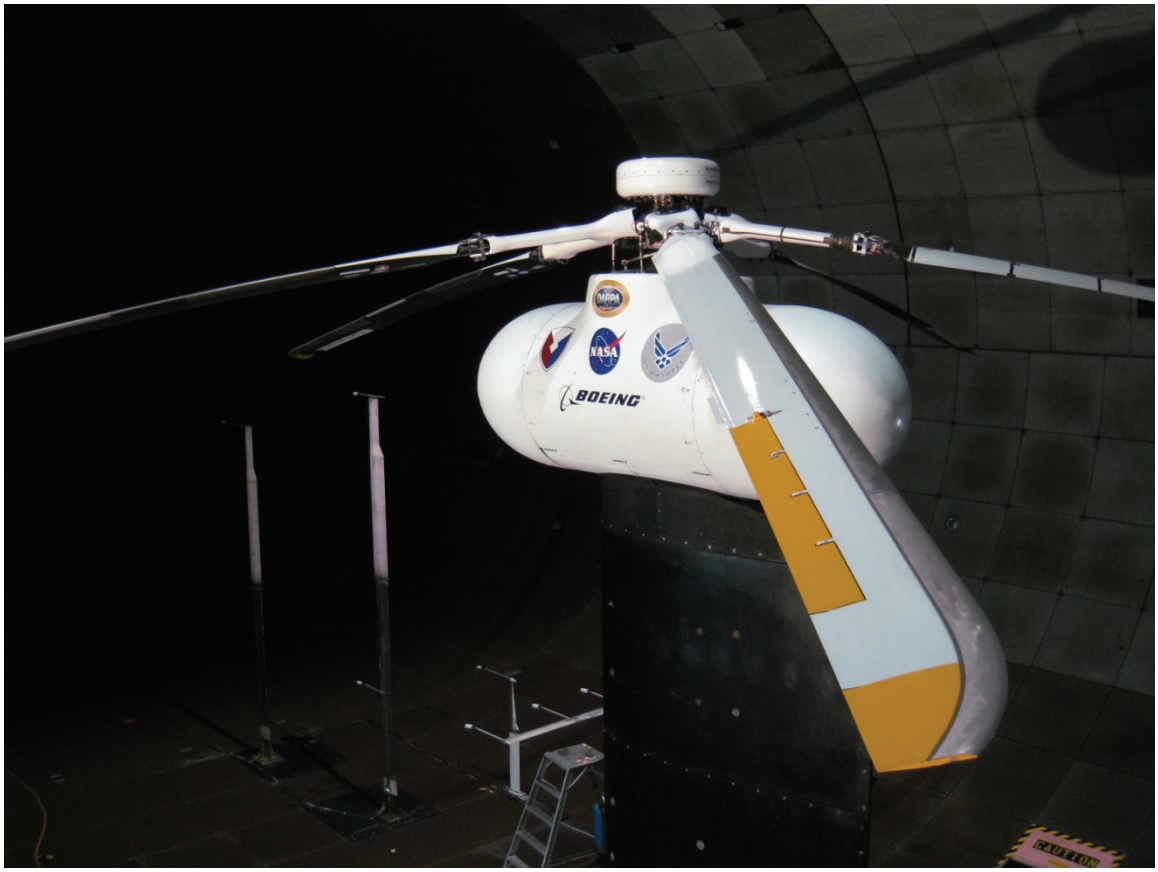

Figure 1. Boeing SMART rotor with active trailing-edge flaps in the NFAC 40- by 80-Foot Wind Tunnel.

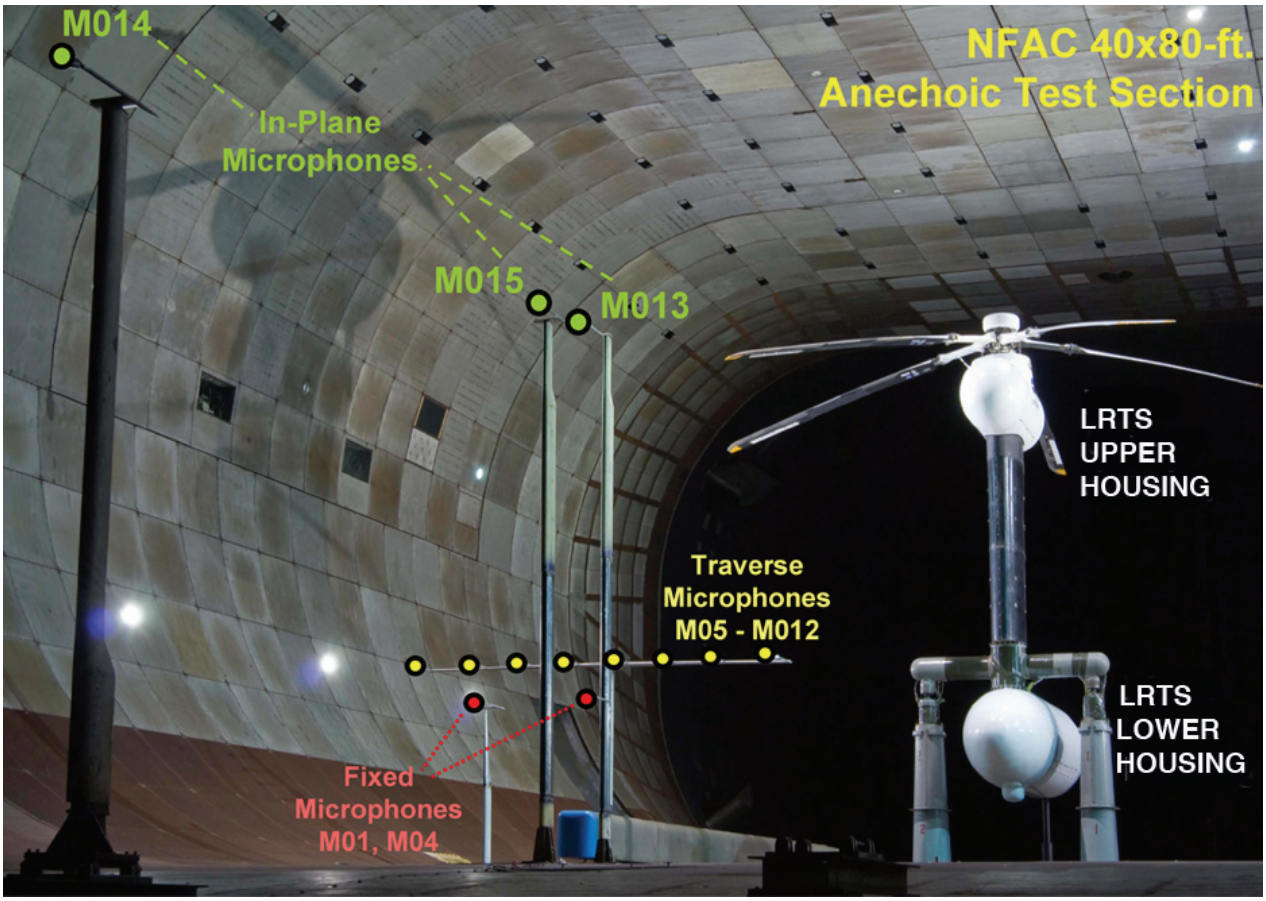

Figure 2. Boeing SMART rotor mounted on the LRTS in the NFAC 40- by 80-Foot Wind Tunnel.

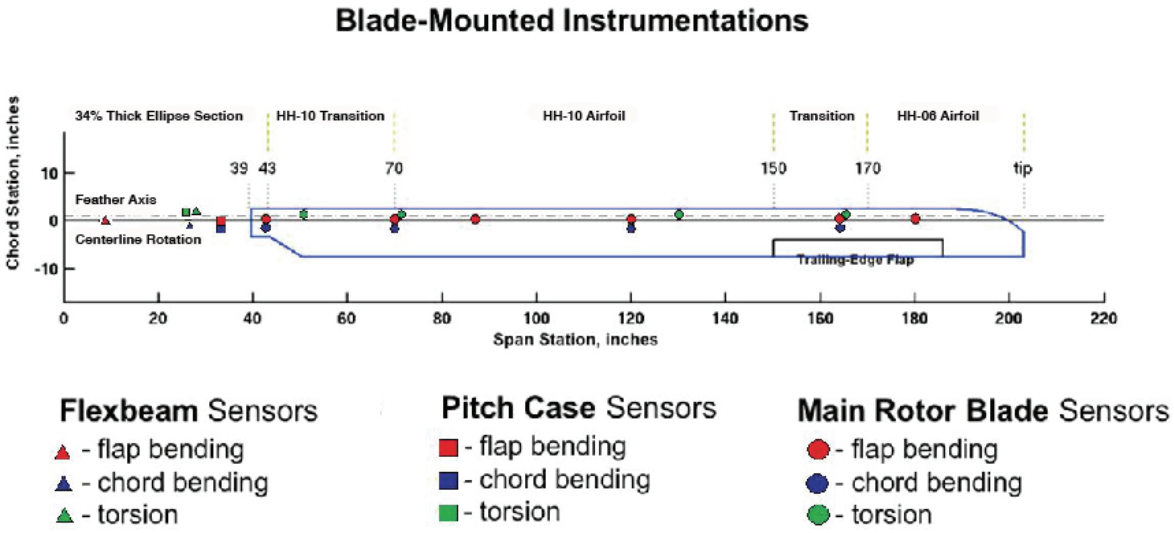

Figure 3. Blade-mounted Instrumentation.

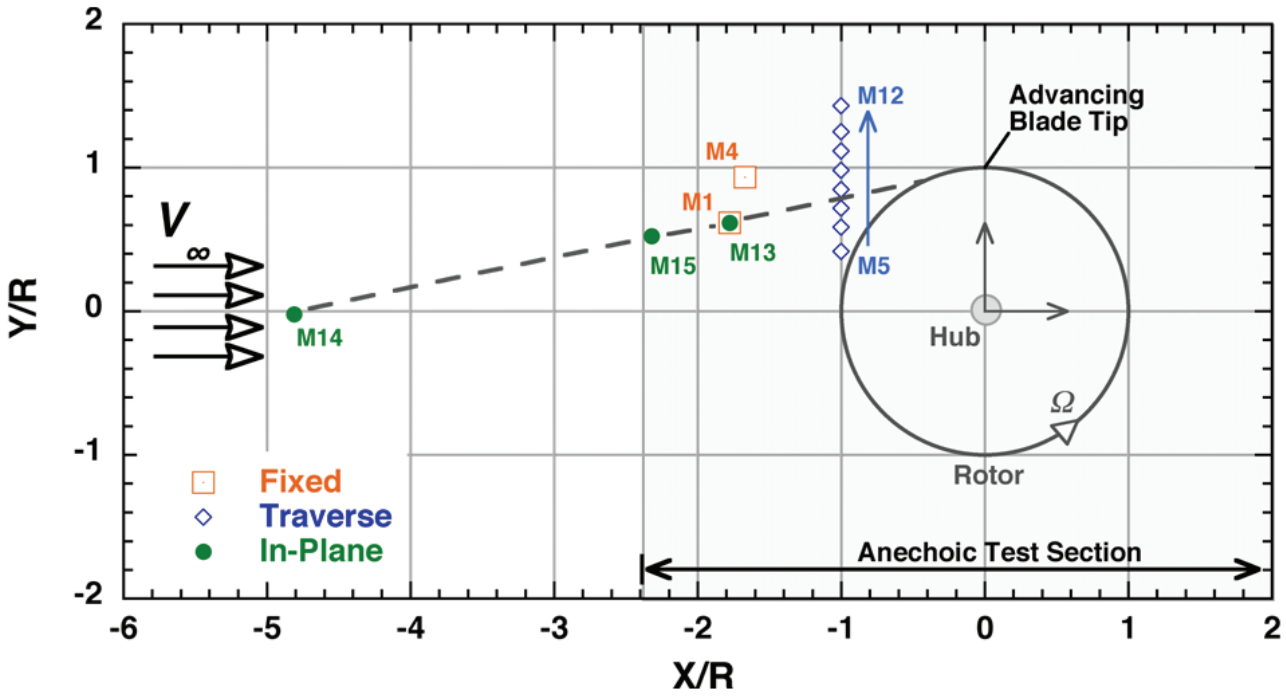

Figure 4. Top view of the test setup of the microphone layout with rotor hub at α_{su} = 0 deg.

APPENDIX A—SPECIFIC TEST SUMMARIES

This appendix briefly describes the specific tests: Rotor Smoothing, Performance, Vibration Reduction, and Control Power. The "Static" and "Dynamic" *parameters* and their *descriptions* (including units and positive directions) are common to all data appendices. These are given below for reference; Appendices B and C contain the actual Trim Static and Trim Dynamic data. Appendices B through K are included in the data DVD.

STATIC DATA PARAMETERS AND DESCRIPTIONS

Channel Name	Description	Units	Positive Direction
VKTS	Tunnel speed	kt	
ALFSC	Corrected angle of attack, Boeing data	deg	aft
HP	Horsepower from rotor torque	HP	
THRUST	Rotor thrust force parallel to the rotor shaft, shaft axes system	lbf	up
COLLA	Rotor collective control input, obtained from the actuator A set of LVDTs, positive nose up	deg	nose up
MTUN	Tunnel Mach number		
CTOS	Rotor thrust coefficient over solidity, parallel to the rotor shaft, shaft axes system		up
LATA	Rotor lateral control input, obtained from the actuator A set of LVDTs, positive nose down at PSI = 0 deg	deg	nose down at PSI = 0 deg
MU	Rotor advance ratio		
MTIP	Tip Mach number		
Flap 1 Amp	Flap 1 maximum angle	deg	t.e. down
LONGA	Rotor longitudinal control input, obtained from the actuator A set of LVDTs, positive nose down at PSI = 90 deg	deg	nose down at PSI = 90 deg
OMR	Rotor tip speed	ft/s	CCW from top
MAT	Rotor advancing tip Mach number		
RPM	Rotor rpm	rpm	CCW from top
ROLLRH	Rotor roll moment obtained from the rotor balance, corrected for weight tare and shaft rotation tare	in-lbf	right down
Flap 1 Phase	Phase angle flap 1 began	deg	CCW zero over tail
PS	Static pressure at tunnel centerline	psfa	
PITCHRH	Rotor pitch moment obtained from the rotor balance, corrected for weight tare and shaft rotation tare	in-lbf	nose up
Flap 1 Harm	Harmonic/s induced into flap controller		
RHO	Air density	$slug/ft^3$	
TORQ	Rotor torque	in-lbf	drag
Q	Corrected tunnel dynamic pressure	psf	
TSR	Tunnel static temperature	deg_R	
SIDERH	Rotor side force obtained from the rotor balance, corrected for weight tare and shaft rotation tare	lbf	right
CSND	Tunnel speed of sound	ft/s	
VISC	Tunnel air viscosity	slug/ft-sec	
DRAGRH	Rotor drag force obtained from the rotor balance, corrected for weight tare and shaft rotation tare	lbf	aft
CPOS	Rotor power coefficient over solidity		

DYNAMIC DATA PARAMETERS AND DESCRIPTIONS

Channel Name	Description	Units	Positive Direction
FLAP1C	Flap 1 Angle (corrected)	deg	t.e. down
ACT1DISP	MR Flap Actuator1 Displacement (feedback), Sta 150	V	aft
ACT1FORCE	MR Flap Actuator1 Force (flap link), Sta 150	lbf	compression
FA1IBCURRENT	Flap Actuator1 Inboard Current	A	
FA1IBVOLTAGE	Flap Actuator1 Inboard Voltage	V	
FA1OBCURRENT	Flap Actuator1 Outboard Current	A	
FA1OBVOLTAGE	Flap Actuator1 Outboard Voltage	V	
MRBLD1CB42P75	MR Blade 1 Chord Bending Sta 42.75	in-lbf	lag
MRBLD1CB70	MR Blade 1 Chord Bending Sta 70	in-lbf	lag
MRBLD1CB120	MR Blade 1 Chord Bending Sta 120	in-lbf	lag
MRBLD1CB164	MR Blade 1 Chord Bending Sta 164	in-lbf	lag
MRBLD1FB42P75	MR Blade 1 Flap Bending Sta 42.75	in-lbf	tip up
MRBLD1FB70	MR Blade 1 Flap Bending Sta 70	in-lbf	tip up
MRBLD1FB87	MR Blade 1 Flap Bending Sta 87	in-lbf	tip up
MRBLD1FB120	MR Blade 1 Flap Bending Sta 120	in-lbf	tip up
MRBLD1FB164	MR Blade 1 Flap Bending Sta 164	in-lbf	tip up
MRBLD1FB180	MR Blade 1 Flap Bending Sta 180	in-lbf	tip up
MRBLD1TOR51	MR Blade 1 Torsion Sta 51	in-lbf	le up
MRBLD1TOR71	MR Blade 1 Torsion Sta 71	in-lbf	le up
MRBLD1TOR130	MR Blade 1 Torsion Sta 130	in-lbf	le up
MRBLD1TOR164	MR Blade 1 Torsion Sta 164	in-lbf	le up
MRFBM1CB26P5	MR Flexbeam 1 Chord Bending Sta 26.5	in-lbf	lag
MRFBM1FB9	MR Flexbeam 1 Flap Bending Sta 9	in-lbf	tip up
MRFBM1TOR26P5	MR Flexbeam 1 Torsion Sta 26.5	in-lbf	le up
MRPC1CB33P25	MR Pitchcase 1 Chord Bending Sta 33.25	in-lbf	lag
MRPC1FB33P25	MR Pitchcase 1 Flap Bending Sta 33.25	in-lbf	tip up
MRPC1TOR25P5	MR Pitchcase 1 Torsion Sta 25.5	in-lbf	le up
MRPLK1LOAD	MR Pitchcase 1 Pitchlink Load	lbf	tension
PITCHRH	Rotor pitch moment obtained from the rotor balance, corrected for weight tare and shaft rotation tare	in-lbf	nose up
ROLLRH	Rotor roll moment obtained from the rotor balance, corrected for weight tare and shaft rotation tare	in-lbf	right down
TORQ	Rotor torque	in-lbf	drag
THRUST	Rotor thrust force parallel to the rotor shaft, shaft axes system	lbf	up
SIDERH	Rotor side force obtained from the rotor balance, corrected for weight tare and shaft rotation tare	lbf	right
DRAGRH	Rotor drag force obtained from the rotor balance, corrected for weight tare and shaft rotation tare	lbf	aft

Rotor Smoothing (Appendices D & E)

Initial rotor tracking was accomplished by adjusting pitch links. No trim tab adjustments were used for tracking. The blades were tracked within ±0.25 in. during hover and checked during forward flight runs. Rotor smoothing using an active trailing-edge flap is achieved by making steady-state inputs to individual flaps. Blades #1 or #2 were selected for the steady state inputs. Using the position control, the flaps were stepped up by 1-deg increments from –3 deg to 3 deg. The effectiveness of this technique was measured using the mean thrust and 1/rev roll and pitch moments resulting from the rotational lift. All test conditions for rotor smoothing are listed immediately below. Not all of the data associated with these conditions have been subjected to the control criteria discussed in the Data Analysis section. Appendices D and E contain rotor smoothing data that *were* subjected to the control criteria.

Rotor Smoothing	Condition	Velocity (knots)	Advance Ratio, μ	Tip Mach Number	Shaft Angle Uncorrected α, deg	Blade Loading, C_T/σ	Harmonic Number
	1	0	0	0.623	–10	0.028	0
	2	82	0.2	0.623	2	0.075	0
	3	124	0.3	0.623	–9.1	0.075	0
	4	124	0.3	0.623	–9.1	0.075	0

Performance (Appendices F & G)

SMART rotor performance data was obtained for several values of advance ratio, rotor shaft angle, and thrust. Rotor performance, defined here as rotor L/D, was studied by varying the 2P flap input from 0–1.5 deg at μ = 0.3. The rotor performance data were obtained with the rotor trimmed for minimum 1P flapping. Two methods of achieving this were investigated: (1) setting flap actuator voltage to zero, and (2) commanding the flap deflection to zero. Both open loop and closed loop feedback control, using a continuous time higher harmonic controller (CTHHC) (ref. 11) were used to drive flap actuation. All test conditions for the performance study are listed immediately below. Not all of the data associated with these conditions have been subjected to the control criteria discussed in the Data Analysis section. Appendices F and G contain performance data that *were* subjected to the control criteria.

Performance	Condition	Velocity (knots)	Advance Ratio, μ	Tip Mach Number	Shaft Angle Uncorrected α, deg	Blade Loading, C_T/σ	Harmonic Number
	1	82	0.2	0.623	2	0.075	n/a
	2	124	0.3	0.623	–9.1	0.075	n/a
	3	124	0.3	0.623	–9.1	0.075	2
	4	124	0.3	0.623	–9.1	0.090	2

Vibration Reduction (Appendices H & I)

Vibration reduction with closed loop feedback of vibratory hub loads was demonstrated using a CTHHC (ref. 11). Numerous active flap frequency sweeps were conducted to obtain data required for the flight controls objective and for determining the parameters for the closed loop CTHHC vibration controllers. Open loop flap 4P, 5P, and 6P inputs with phase sweeps were used to establish the effectiveness of the flap in reducing vibratory hub loads. The flaps were driven using open loop voltage commands without position feedback control. The effectiveness of the active flap to modify the aerodynamic loading and reduce vibratory hub loads was evaluated at two flight conditions, descent ($\mu = 0.2$, $\alpha = 2$ deg) and level flight ($\mu = 0.3$, $\alpha = -9.1$ deg). All test conditions for vibration reduction are listed immediately below. Not all of the data associated with these conditions have been subjected to the control criteria discussed in the Data Analysis section. Appendices H and I contain vibration reduction data that *were* subjected to the control criteria.

Vibration Reduction	Condition	Velocity (knots)	Advance ratio, μ	Tip Mach Number	Shaft Angle Uncorrected α, deg	Blade Loading, C_T/σ	Harmonic Number
	1	82	0.2	0.623	2	0.075	2,3,4,5,6
	2	82	0.2	0.623	2	0.075	closed loop
	3	124	0.3	0.623	–9.1	0.075	2,3,4,5,6
	4	124	0.3	0.623	–9.1	0.075	closed loop

Control Power (Appendices J & K)

Control power from the active flaps was evaluated by applying equivalent steady-state collective, lateral, or longitudinal cyclic flap deflections and observing the resulting changes in normal force, roll, and pitch moment. Flaps were controlled either by individual blade control (IBC), specifying harmonic and phase, or through software implementation of a virtual swashplate (VSP), using amplitude and collective, longitudinal, and lateral cyclic commands. Flap deflections were generated from –3 to 3 deg using the VSP software for flap inputs on each blade, or by applying steady offset for collective 1P/90 deg for roll and 1P/180 deg for pitch inputs (IBC). Results for position control flap inputs, both VSP and IBC, and comparable swashplate inputs were obtained at $\mu = 0.2$ for level flight and descent, and for level flight at $\mu = 0.3$. All test conditions for the control power study are listed immediately below. Not all of the data associated with these conditions have been subjected to the control criteria discussed in the Data Analysis section. Appendices J and K contain control power data that *were* subjected to the control criteria.

Control Power	Condition	Velocity (knots)	Advance Ratio, μ	Tip Mach Number	Shaft Angle Uncorrected α, deg	Blade Loading, C_T/σ	Harmonic Number
	1	82	0.2	0.623	–5.5	0.075	0,1
	2	82	0.2	0.623	2	0.075	0,1
	3	124	0.3	0.623	–9.1	0.075	0,1

REFERENCES

1. Murrill, R. J.; Hamilton, B. K.; Anand, V. R.; Lauzon, D. M.; and Tuttles, B.: Bearingless Main Rotor Whirl Test: Design, Analysis, and Test Results. American Helicopter Society 49th Annual Forum Proceedings, St. Louis, MO, May 19–21, 1993.
2. McNulty, M.; Jacklin, S.; and Lau, B.: A Full-Scale Test of the McDonnell Douglas Advanced Bearingless Rotor in the NASA Ames 40- by 80- Foot Wind Tunnel. American Helicopter Society 49th Annual Forum Proceedings, St. Louis, MO, May 19–21, 1993.
3. Jacklin, S. J.; Lau, B. H.; Nguyen, K. Q.; Smith, R. L.; and McNulty, M.J.: Full-Scale Wind Tunnel Test of the McDonnell Douglas Five-Bladed Advanced Bearingless Rotor: Performance, Stability, Loads, Control Power, Vibration, and HHC Data. American Helicopter Society Aeromechanics Specialists' Conference, San Francisco, CA, January 19–21, 1994.
4. Nguyen, K.; McNulty, M.; Anand, V.; and Lauzon, D.: Aeroelastic Stability of the McDonnell Douglas Advanced Bearingless Rotor. American Helicopter Society 49th Annual Forum Proceedings, St. Louis, MO, May 19–21, 1993.
5. Kottapalli, S.: Enhanced Correlation of SMART Active Flap Rotor Loads. AIAA paper no. 2011-1874, 52nd AIAA/ASME/ASCE/AHS/ASC Structures, Structural Dynamics, and Materials Conference, Denver, CO, April 4–7, 2011.
6. Newman, D.; Doligalski, T.; and Minniti, R.: Advances in Modeling and Simulation of Rotorcraft Noise and Associated Impacts on Survivability. Presented at the 26th Army Science Conference, Orlando, FL, Dec. 2008.
7. Lau, B. H.; Obriecht, N.; Gasow, T.; Hagerty, B.; Cheng, K. C.; and Sim, B.: Boeing-SMART Test Report for DARPA Helicopter Quieting Program. NASA TM 2010-216404, Sept. 2010.
8. Straub, F. K.; Anand, V. R.; Birchette, T. S.; and Lau, B. H.: Wind Tunnel Test of the SMART Active Flap Rotor. American Helicopter Society 65th Annual Forum Proceedings, Grapevine, TX, May 27–29, 2009.
9. Sim, B. W.; JanakiRam, R. D.; Barbely, N. L.; and Solis, E.: Reduced In-Plane, Low-Frequency Noise of an Active Flap Rotor. Presented at the American Helicopter Society 65th Annual Forum, Grapevine, TX, May 2009.
10. JanakiRam, R. D.; Sim, B. W.; Kitaplioglu, C.; and Straub, F. K.: Blade-Vortex Interaction Noise Characteristics of a Full-Scale Active Flap Rotor. Presented at the American Helicopter Society 65th Annual Forum, Grapevine, TX, May 2009.
11. Hall, S. R.; Anand, V. R.; Straub, F. K.; and Lau, B.H.: Active Flap Control of the SMART Rotor for Vibration Reduction. American Helicopter Society 65th Annual Forum Proceedings, Grapevine, TX, May 27–29, 2009.
12. Straub, F. K. and Anand, V. R.: Whirl Tower Test and Analysis of the Smart Material Actuated Rotor Technology (SMART) Active Flap Rotor. American Helicopter Society 63rd Annual Forum Proceedings, Virginia Beach, VA, May 1–3, 2007.
13. Straub, F. K., et al.: Development and Whirl Tower Test of the SMART Active Flap Rotor. SPIE Conference on Smart Material and Structures, San Diego, CA, 2004.

14. Kottapalli, S. and Straub, F. K.: Correlation of SMART Active Flap Rotor Loads. American Helicopter Society 65th Annual Forum Proceedings, Grapevine, TX, May 27–29, 2009.

15. Kottapalli, S.: Low-Speed and High-Speed Correlation of SMART Active Flap Rotor Loads. American Helicopter Society Aeromechanics Specialists' Conference, San Francisco, CA, January 20–22, 2010.

16. Straub, F. K.; Silverthorn, L.; Anand, V.; JanakiRam, R.; Birchette, T.; and Meyers, P.: SMART Rotor Wind Tunnel Test Report. Boeing Company Subsonic Rotary Wing Technology Development, Feb. 2010.

17. Straub, F. and Anand, V. R.: SMART Rotor Extended Wind Tunnel Test Plan Draft and Closed Loop Control Methodologies Report. Report L9S7-05-DTP-08001, CDRL 5-2, Flight Technology Technical Note FTN-2008-010, The Boeing Company, Feb. 2008.

18. Anand, V. R. and Straub, F.: SMART Rotor Wind Tunnel Test-Software Plan. Report L9S7-03-FTP-08002, CDRL 3-2, Flight Technology Technical Note FTTN-2008-003, The Boeing Company, Jan. 2008.

19. Anand, V.; JanakiRam, R.; Straub, F. K.; and Macaraeg, D.: SMART Rotor Wind Tunnel Test-Data and Flap Control Plan Draft. Boeing Company Subsonic Rotary Wing Technology Development, Aug. 2007.